Chapter VI

FINITE-DIFFERENCE MODELING AND MIGRATION IN MEDIA WITH LATERALLY VARIABLE ATTENUATION AND VELOCITY

The expressions derived in the previous chapters make it possible to describe wave propagation in rocks for monochromatic waves, including the effects of absorption. While the theory for the finite-difference modeling of waves in the frequency domain has been developed in detail [Claerbout, 1971, 1976], its use appears to have been rather limited. As the properties of the earth may be considered time-invariant for the duration of seismic experiments and linear at seismic amplitudes, no generality is lost by Fourier transforming over time. There are several advantages in working in the frequency domain. Each Fourier component of the seismogram may be propagated separately, which can simplify manipulations of large datasets compared to time-domain methods. A time shift over a non-integer number of sampling intervals consists in the frequency domain of a simple multiplication. Perhaps the greatest advantage of the frequency domain is that all time derivatives are evaluated exactly by a simple multiplication. This becomes increasingly important as more accurate equations involving higher time derivatives are used. This also makes it possible to include the effects of anelasticity at little or no additional cost.

Wave-Field Extrapolation

It is shown by Claerbout [1976, p. 196] that the scalar wave equation for constant density

$$P_{zz} + P_{xx} = \frac{1}{v^2} P_{tt} \tag{6.1}$$

where the subscripts denote partial derivatives, becomes

$$R_{zz} + R_{xx} + 2i\bar{m}R_z + (m^2-\bar{m}^2)R = 0 \tag{6.2}$$

when R is defined by

$$R(x,z,\omega) = e^{i\bar{m}z}\,\bar{P}(x,z,\omega) \tag{6.3}$$

$$\bar{P}(x,z,\omega) = \int_{-\infty}^{\infty} P(x,z,t)e^{-i\omega t}\,dt \tag{6.4}$$

$$m = -\frac{\omega}{v} \tag{6.5}$$

$$\bar{m} = -\frac{\omega}{\bar{v}} \tag{6.6}$$

In the derivation of this result, $\bar{v}$ has been assumed to be independent of x and z, while v may be a function of both x and z. Since we are using a minus sign in the forward Fourier transform [Bracewell, 1965], the signs in equations (6.5) and (6.6) are different from those used by Claerbout [1976].

The R_{zz} term is eliminated if each term in equation (6.2) is differentiated with respect to z, multiplied by $i/2\bar{m}$, and added to the original equation. The result is

$$\frac{i}{2\bar{m}}R_{zzz} + \frac{i}{2\bar{m}}R_{xxz} + R_{zz} + 2i\bar{m}R_z + \frac{i}{2\bar{m}}(m^2-\bar{m}^2)R_z \tag{6.7}$$

$$+ (m^2-\bar{m}^2)R + \frac{im}{\bar{m}}\frac{dm}{dz}R = 0$$

It should be noted that we have not made any approximations yet: equation (6.7) is simply the scalar wave equation in a shifted coordinate frame.

For waves traveling in approximately the same direction as the coordinate frame is shifted, R_{zzz} should be small in relation to the other terms. If it is dropped, the result

$$\frac{i}{2\bar{m}}R_{xxz} + R_{zz} + 2i\bar{m}R_z + \frac{i}{2\bar{m}}(m^2-\bar{m}^2)R_z + (m^2-\bar{m}^2)R + \frac{im}{\bar{m}}\frac{dm}{dz}Q = 0 \tag{6.8}$$

will be first order in z. The dispersion relation is shown in figure 6.1. As shown in figure 6.1, the dispersion relation for equation (6.8) starts to

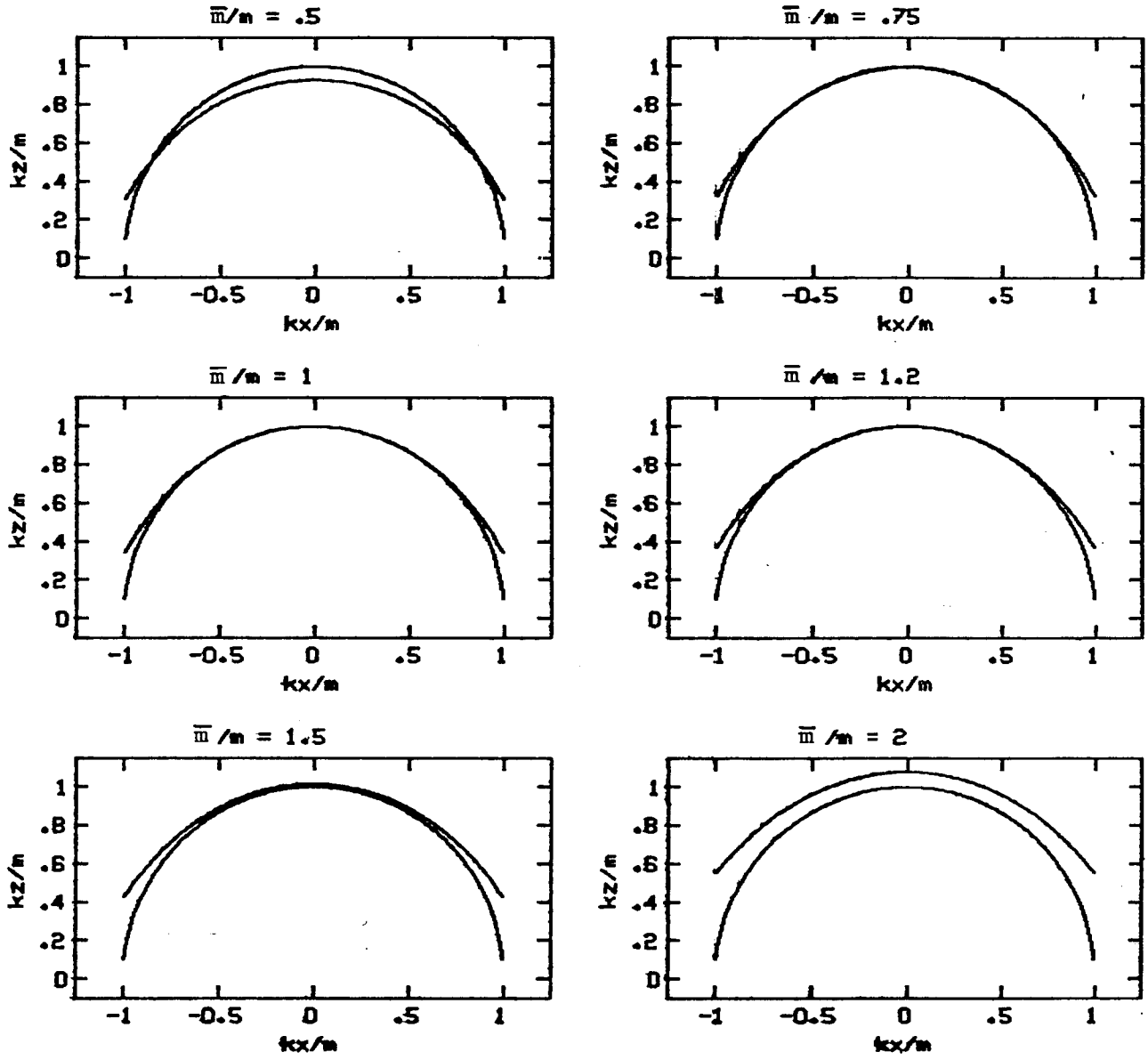

FIG. 6.1. The dispersion relation for equation (6.8). Each plot shows the k_z/m as a function of k_x/m. For comparison the semicircle is also shown. The accuracy of equation (6.8) is quite acceptable for $0.7m < \bar{m} < 1.5m$.

deviate significantly from the correct value when $\bar{m}$ and m differ by more than 50 percent.

In many cases this is not a serious limitation. I have used equation (6.8) extensively to model and migrate seismic sections, without any difficulties. If it is assumed that the coefficients in equation (6.1) are locally constant, one may set $m = \bar{m}$ and then apply a time shift at each depth step. This assumption that the coefficients are locally constant is commonly made, e.g. when a wave equation is derived to satisfy a particular dispersion relation.

Thus one can get the wave field $\bar{P}(z+\Delta z)$ from $\bar{P}(z)$ by setting

$$R(z) = \bar{P}(z) \tag{6.9}$$

and solving

$$\frac{i}{2m(x,z)} R_{xxz} + R_{xx} + 2im(x,z)R_z = 0 \tag{6.10}$$

for $R(z+\Delta Z)$, and then applying the time shift

$$\bar{P}(z+\Delta z) = \exp\left[im(x,z)\Delta z\right]R(z+\Delta z) \tag{6.11}$$

Equation (6.10) is simpler to code than equation (6.8) and has a more accurate dispersion relation, but does not treat the effects of velocity gradients as accurately as equation (6.8). Both equations fit on the finite-difference star described by Claerbout [1976, p. 184-189] and may be solved using the Crank-Nicolson scheme.

Exploding Reflector Model

Most migration and modeling techniques use an imaging principle based on the exploding reflector model. Two basic assumptions are involved. The first is that the the CMP stacked section is equivalent to a zero-offset section. The second assumption is that a zero-offset section may be modeled by placing

sources on all the reflectors at t = 0 and continuing the resulting wave field to the surface, using half the true velocity. This has been discussed by various authors [e.g. Stolt, 1978], but it is usually assumed that the velocity depends only on depth. We will explore the extent to which the exploding reflector model is valid when lateral variations in velocity are present. The results may be extended to non-zero offsets; this leads to an accurate method for the computation of synthetic seismograms for all offsets. For simple reflectivity structures this method is very economical.

Theory

We will assume that the reflection seismogram can be approximated by a distribution of point scatterers, imbedded in a variable velocity medium. This assumption is valid when the reflection coefficients are small and independent of the angle of incidence. When this is the case, seismograms can be computed for arbitrary reflectivity structures by superposition of the seismograms resulting from each reflector point. The seismogram, ${}_sS_g$, recorded at g from a source at s, may be considered as a convolution of the shot waveform W (as it would be recorded by the recording instrument), the propagation from the source to the reflector ${}_sP_r$, the reflectivity R and the propagation from the reflector to the geophone ${}_rP_g$. In the frequency domain this may be written as follows:

$$ {}_sS_g = W \; {}_sP_r \; R \; {}_rP_g \tag{6.12} $$

In the case of zero offset reciprocity implies that

$$ {}_sP_r = {}_rP_g \tag{6.13} $$

and

$$ {}_gS_g = W \; R \; {}_rP_g^2 \tag{6.14} $$

Reciprocity may also be used to obtain nonzero offsets when ${}_rP_g$ is known

for all reflector points and surface locations. For a single point scatterer this requires no more computation than the upward continuation of the wave field due to a point source at depth. When the velocity structure is such that ${}_rP_g$ consists of a single spike, with traveltime t_o and amplitude A_g, it is easy to see that ${}_rP_g^2$ is a spike arriving at $2t_o$ with an amplitude A_o^2. Thus one may approximate ${}_rP_g^2$ by stretching ${}_rP_g$ and applying a time-dependent gain to correct for geometric spreading.

The condition that ${}_rP_g$ be a spike is not necessary in all cases - for example, if the rate of dissipation is proportional to frequency (constant Q) a plane-wave pulse is broadened in a homogeneous medium such that the seismogram at any distance is obtained by a stretching and scaling of a single seismogram [Kjartansson, 1979]. Because of the frequency-dependence of the velocity, the scaling factor is not exactly proportional to distance. This does not apply for other dissipation laws, such as that treated by Ricker [1953, 1977].

The observed seismogram is a linear function of the reflectivity in the subsurface (for small reflection coefficents). The convolution of a trace on itself is a non-linear operation and must therefore be performed for each reflector point separately. The time stretching is a linear operation so it can be performed for all the traces and reflectors together, implicitly by using half the true velocity. When a linear operator such as the wave equation is used to compute ${}_rP_g$, a great saving in computational effort can result from superposing the reflectors before the wave extrapolation.

The convolution cannot be replaced by time stretching when more than two raypaths connect the reflector and the surface point. This can happen when $\partial^2 v/\partial x^2 \neq 0$ or when the interfaces between layers of different velocities are curved.

Implementation

Thus, when modeling a zero-offset section on the computer using the exploding reflector model, one can start with a blank upgoing wave field below the lowest reflector, then use equations (6.9), (6.10) and (6.11) to continue the wave field up towards the surface. Since a delta function at t=0 has a

Fourier transform that is simply a constant, independent of frequency, one can then model the exploding reflectors by adding the reflection coefficient to all of the frequencies, at each z-step. The time section is then obtained by inversely Fourier transforming the results at the surface.

Migration of zero-offset data is simply the inverse of the above: one starts by Fourier transforming the time section, and then continuing each frequency down, using either a negative v or Δz. The value of the wave field at t=0 is then extracted at each depth by summing over the real part of all the frequencies. An optional step that removes the effect of the wraparound in the FFT is to then subtract the value of the reflector from the wave field.

Both modeling and migration can be performed by taking one frequency at a time through all the z-steps, or taking all the frequencies through one z-step at a time. It is, however, only possible to subtract the reflectors from the migrated wave field when all the frequencies are taken together. In situations where both the reflector and velocity map, and the Fourier transform of the wave field, are too large to fit in the main memory of the computer, disk input and output are minimized by using some combination of the above -- that is, either taking as many frequencies as will fit into memory through all the z-steps, or keeping as much of the velocity and reflector structure as fits in memory, while taking all the frequencies through that part of the structure. Using this last arrangement we have been able to take full advantage of the speed of the SEP array processor for migrations of several hundred traces of COCORP data [Lynn et al. 1979].

Examples

We will show two such examples. Figure 6.2 shows the exploding reflector seismogram for a point source near a vertical interface. The velocity on the left of the interface is one-third what it is on the right. The depth of the point scatterer is 5 times its distance from the vertical interface. Figure 6.3 shows the result computed using equation (6.3) for the same earth structure. The strongest arrival on figure 6.3 is not present at all in the exploding reflector approximation. Note also that the relative amplitudes are different between the two figures. Figure 6.4 shows the raypaths included in figures 6.2 and 6.3. The velocity structures used in these figures are

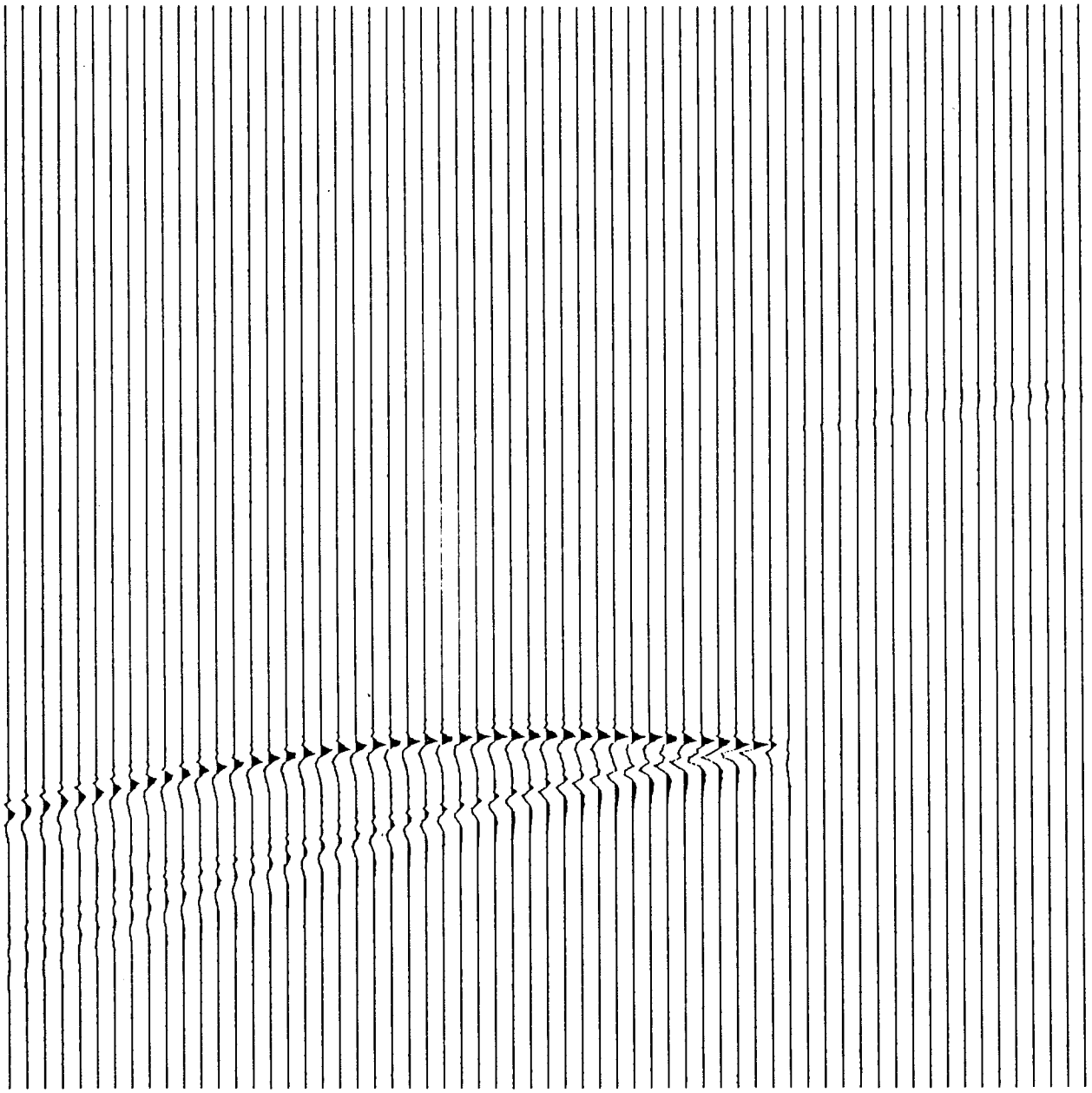

FIG. 6.2. Exploding reflector zero-offset section for a point scatterer at a depth of five times its distance from a vertical velocity contrast of 3 to 1. Computed using monochromatic 45-degree wave equation. Raypaths are shown in figure 6.4a,b.

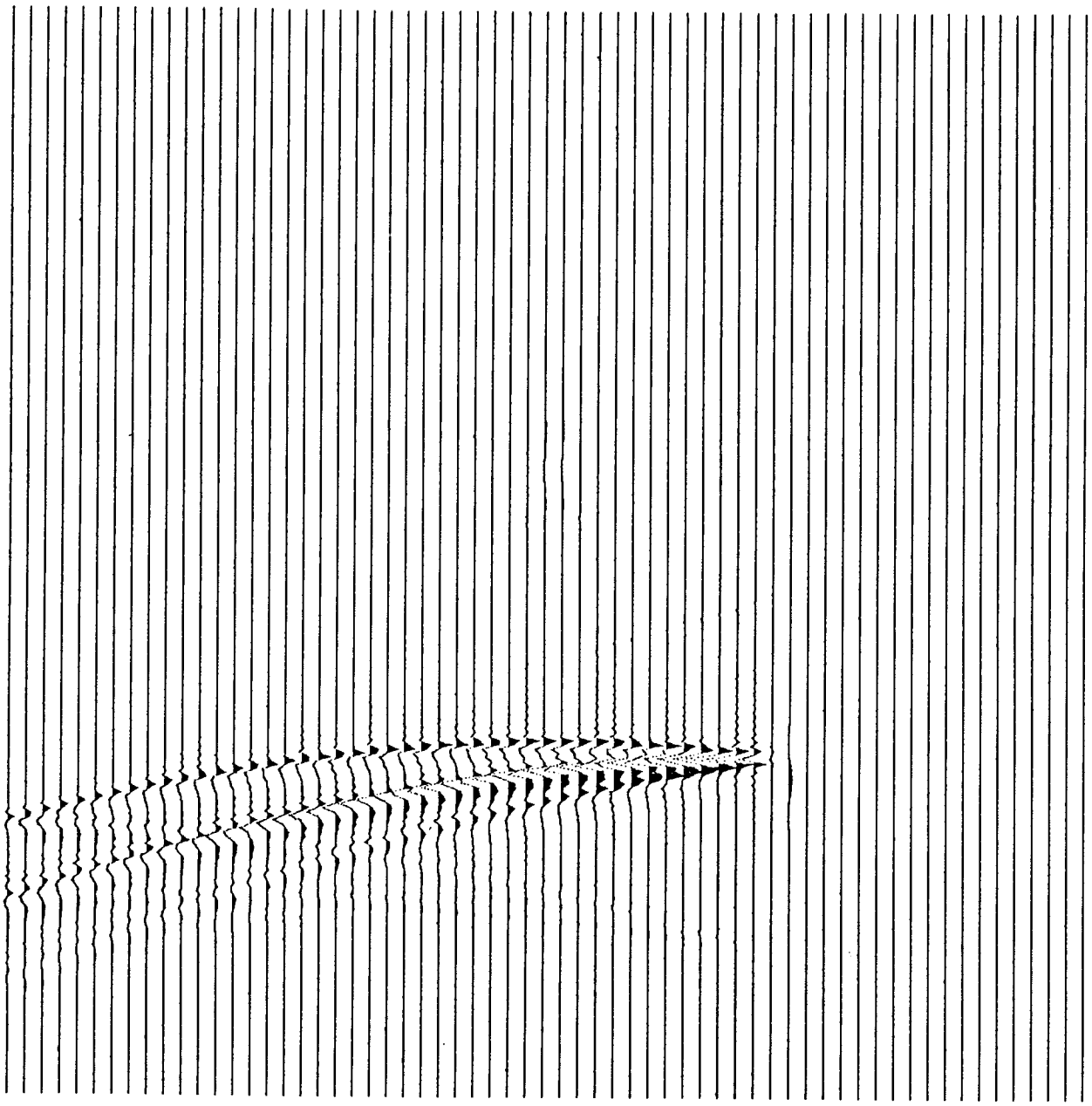

FIG. 6.3. Zero-offset section for same earth model as figure 6.2, computed using equation (6.3). All the raypaths shown in figure 6.4 are now included.

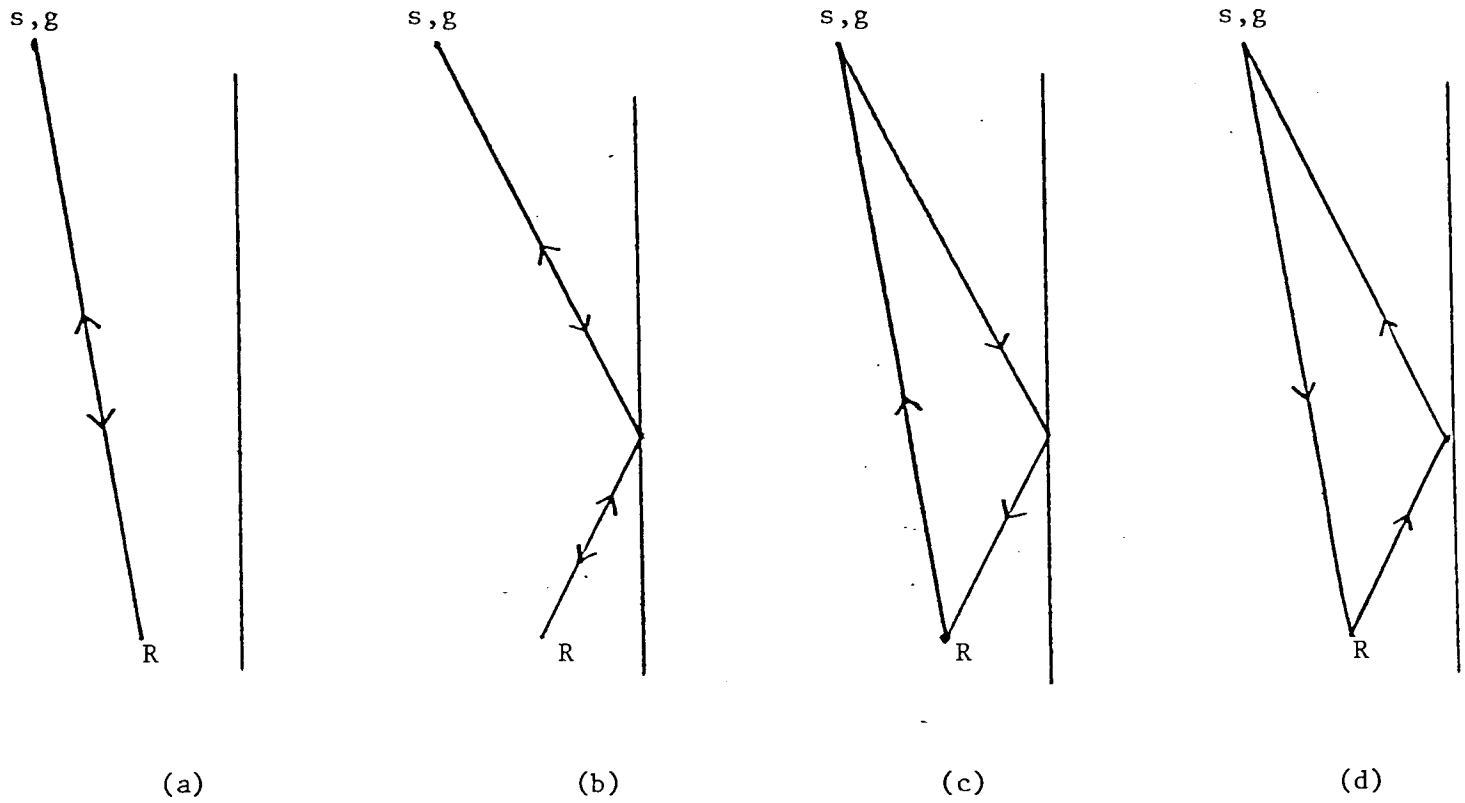

FIG. 6.4. Raypaths for the model in figures 6.2 and 6.3. The exploding reflector model includes only (a) and (b).

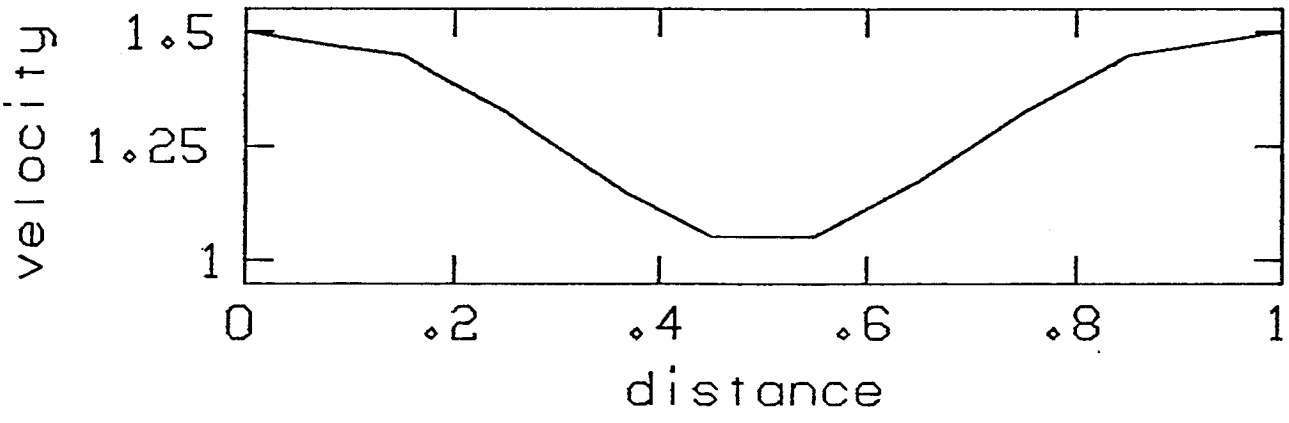

FIG. 6.5. Velocity along the sections in figures 6.6 and 6.7. Velocity is independent of depth.

probably not too realistic from a geologic point of view. Figure 6.5 shows a somewhat more realistic velocity model. For computational convenience we have assumed a velocity that is independent of depth, but very similar effects would be expected for point scatterers below a curved interface between two layers with different velocities, e.g. below a depression in the seafloor. Figure 6.6 shows the exploding reflector result for the velocity function shown in figure 6.5. The source is at a depth that is 1.3 times the width of the computed model. Figure 6.7 shows the correct zero-offset section. As before there are significant differences.

Attenuation

A first-order property of all materials, especially rocks, is the absorption of elastic energy, and the resulting change in the shape of transient waveforms. Most available data is consistent with the assumption that the energy is absorbed by a linear process, and that the energy loss per cycle is independent of frequency. In Chapter II we have seen that these conditions are satisfied by a model that implies a complex, frequency-dependent velocity of the form

$$v = v_0(i\omega)^{\gamma} \tag{6.15}$$

where γ is related to the seismic quality factor Q by

$$\frac{1}{Q} = \tan(\pi\gamma) \tag{6.16}$$

The possible range for γ is $0 < \gamma < \frac{1}{2}$ and for Q is $\infty > Q > 0$. The limiting cases correspond to classical elasticity and Newtonian viscosity. Since the coefficients in the Crank-Nicolson scheme are complex, even for a purely elastic model, the only additional computation, which results from the substitution of equation (6.14) into either (6.5) or (6.6), is in the computation of the coefficients. Appendix B contains FORTRAN listings of an in-core version of a zero-offset diffraction program, which can handle arbitrary velocity and Q structures and the corresponding migration program. Except for the input and output routines, these programs should run on other FORTRAN systems.

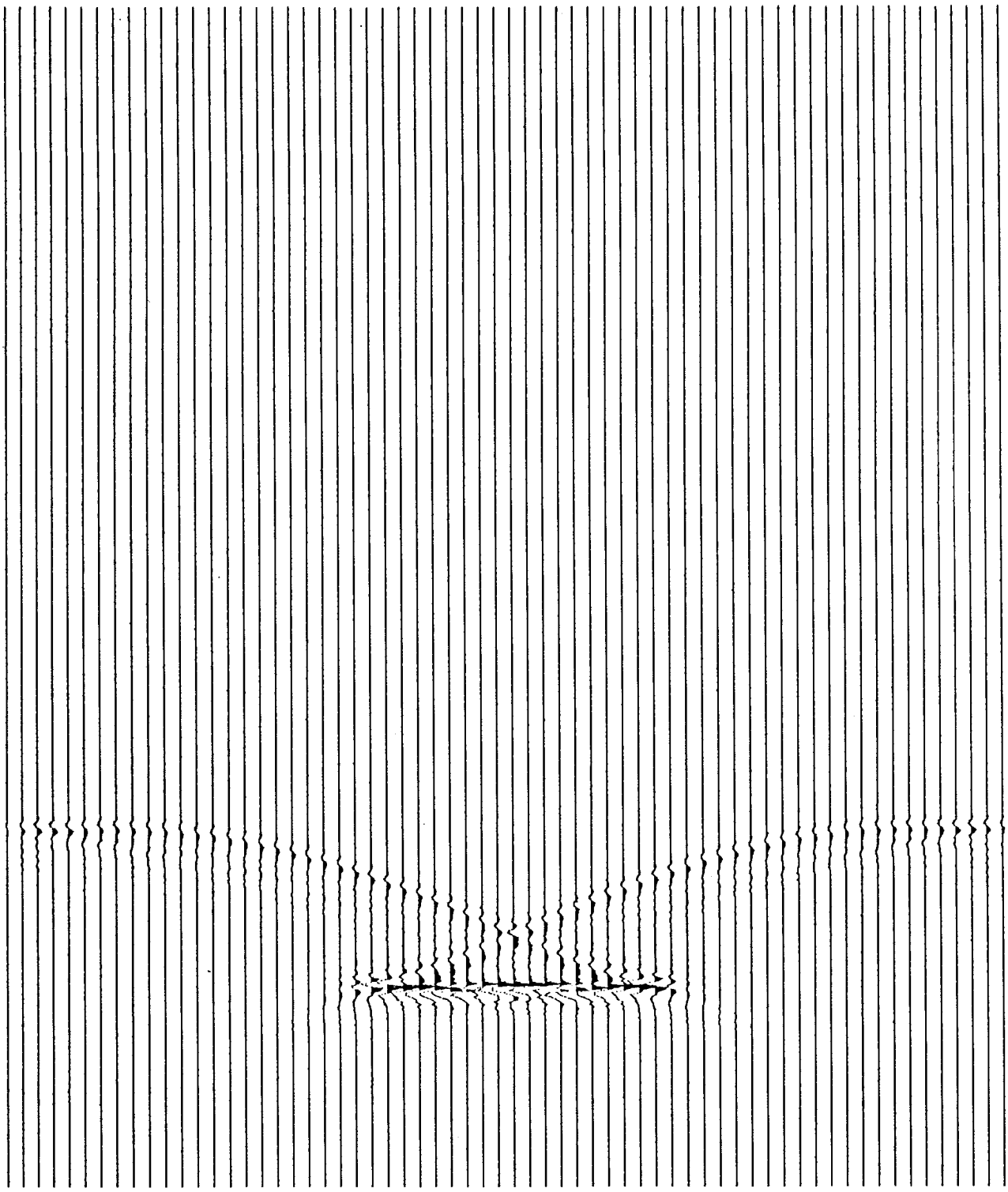

FIG. 6.6. Exploding-reflector-model zero-offset section for a point scatterer at a depth of 1.3 times the width of the section. Velocity is independent of depth and varies as shown in figure 6.5 along the section.

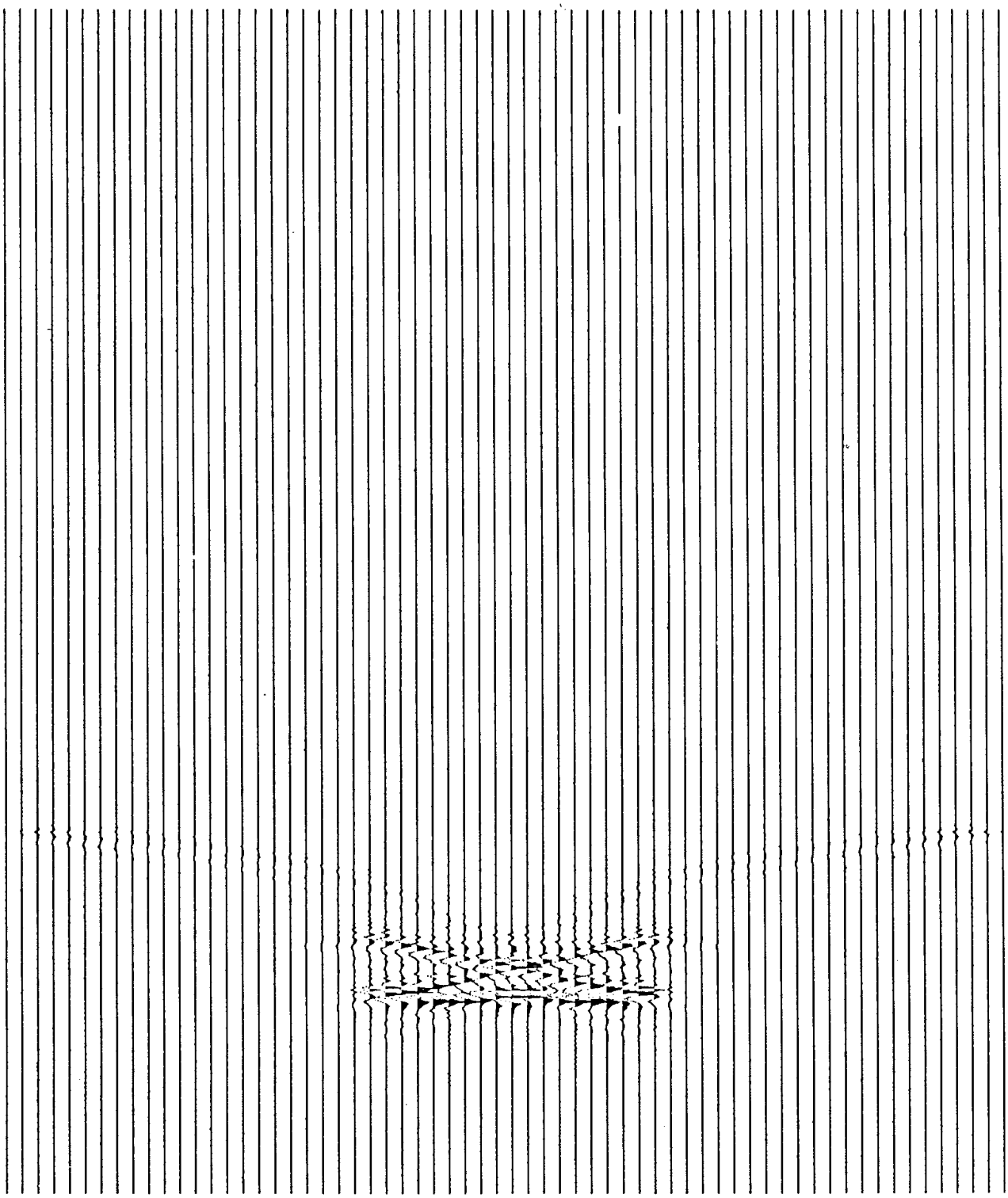

FIG. 6.7. Zero-offset section computed using equation (6.3) for the same earth structure as in figure 6.6.

Figures 6.8-6.11 show examples of outputs produced by these programs, as well as the large dataset array processor versions.

Discussion

It is routine practice [e.g. Burdick and Helmberger, 1978] in the computation of synthetic earthquake seismograms, to compute a seismogram for a purely elastic earth model, and then convolve the result with a response function of the kind presented in Chapter II. This is valid when all the arrivals present on the seismogram have suffered the same amount of attenuation, but is not even approximately valid for reflection seismograms unless it is assumed that all the attenuation takes place in the near-surface layers. Since the waveforms, especially at shorter periods, are often dominated by the attenuation impulse response, it seems worthwhile to include attenuation in the modeling of seismic sections.

Similarly, removal of the attenuation effects, along with the diffractions, in the migration of seismic data, should help isolate the path-independent source waveform, and thus contribute to increasing the resolution of the results. However, the removal of attenuation effects is an inherently unstable process, especially in the presence of noise, so careful filtering of the high frequencies is required, and the results are likely to be sensitive to the quality and processing history of the data. An alternative discussed by Robinson [1979], is to remove only the phase shifts caused by anelasticity dispersion; this may be valuable in obtaining a zero-phase output in deconvolution.

Although an understanding of the seismic attenuation may help us get sharper pictures of the subsurface, that is not the only reason for trying to measure and model it. There are both laboratory [Winkler and Nur, 1979] and theoretical reasons, such as given in Chapter V and by Mavko and Nur [1979], to believe that there is some unique information about the lithology and such parameters as the temperature, porosity, pore pressure, and the amount of saturation that can be extracted from a knowledge of the seismic attenuation parameters, especially when they are integrated with other geophysical information. None of the methods that have been discussed in this chapter are applicable to the problem of estimating Q directly from data. The ability to

compute accurate synthetic seismograms for trial models of the Q structure should be valuable in comparing the various methods for estimating Q and establishing the validity of the results.

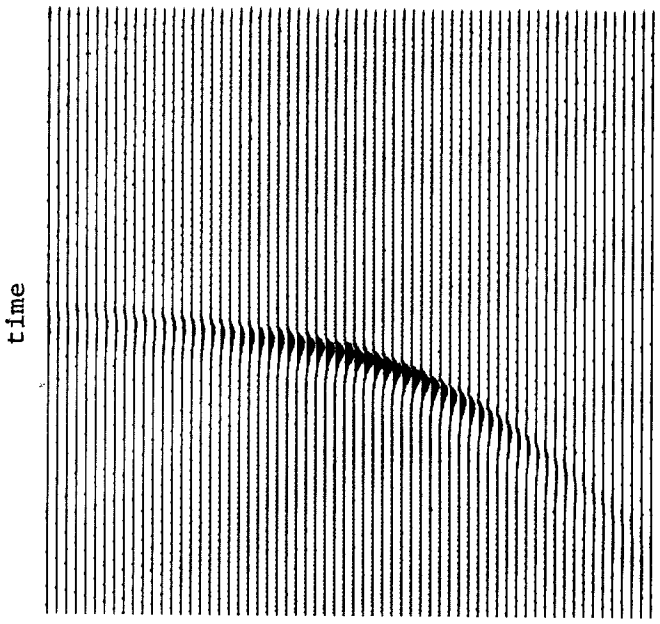

6.8a

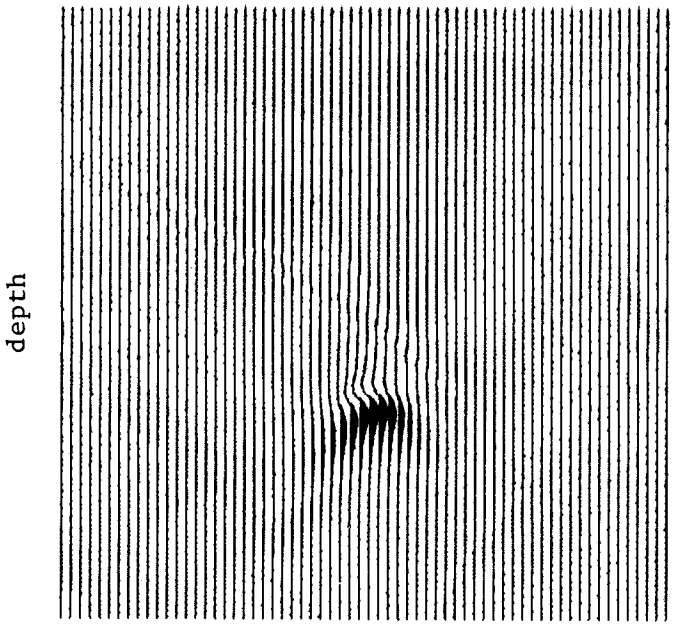

6.8b

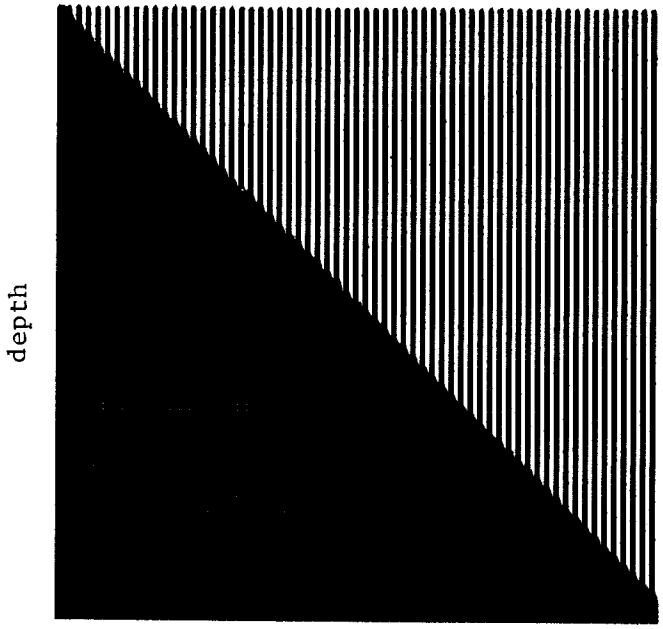

6.8c

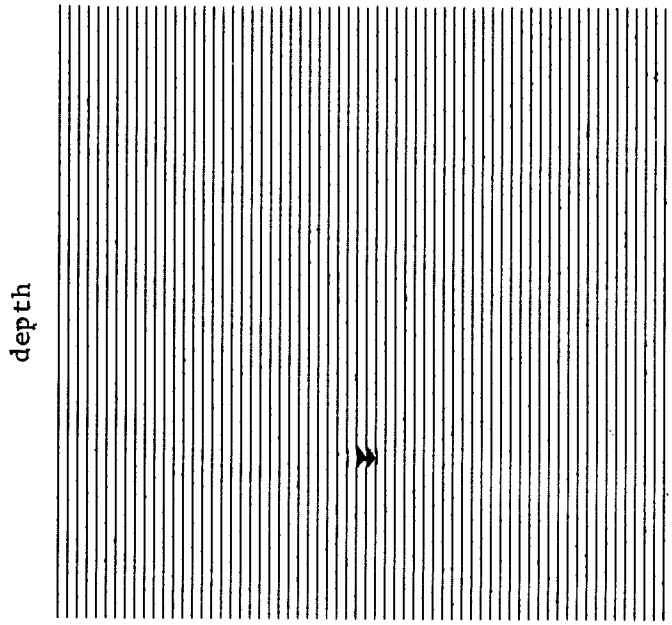

6.8d

FIG. 6.8. Modeling and migration using the programs listed in appendices. The zero-offset section observed at the surface from the reflector shown in 6.8d, for the velocity structure shown in 6.8c, is shown in 6.8a. Anelasticity with Q = 20 was used. The velocity at a unit frequency is 1 in the upper layer and 2 below. The result of a migration of the section in 6.8a is shown in 6.8b. Most of the loss in resolution is because anelasticity was included in the forward calculation, but not in the migration. Parameters used were as follow: 128 timepoints, 64 traces, 64 depthpoints, Δt of 0.06, Δz of 0.06, and Δx of 0.1.

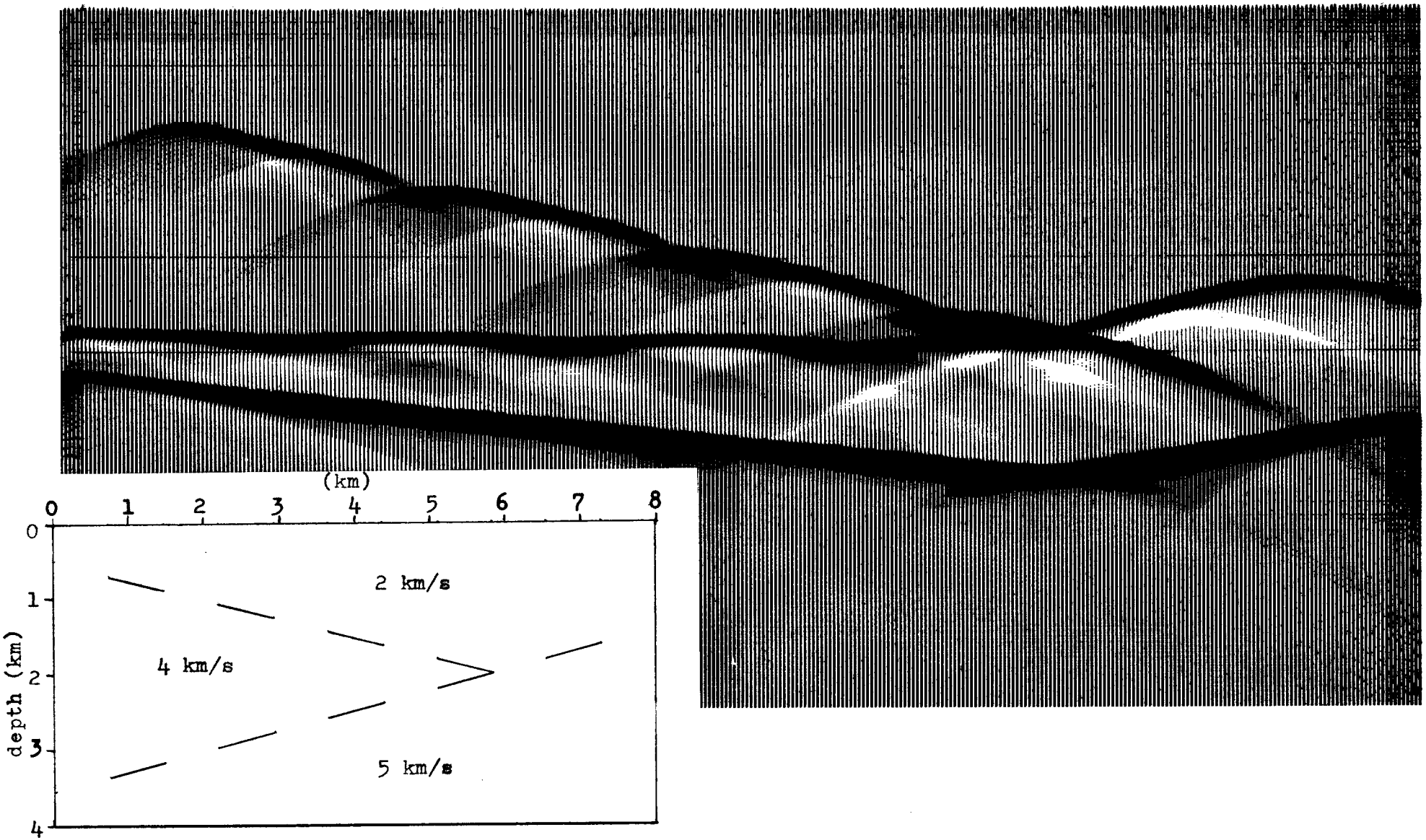

FIG. 6.9. A zero-offset section for the reflector and velocity structure shown, with Q = 40. Total time displayed is four seconds. Velocities shown are for a reference frequency of approximately 1 Hz. The calculation included 330 traces, 320 depth steps and 512 complex frequencies or 1024 timepoints. A gain proportional to $t^{1/2}$ was applied before plotting. The traces are clipped to 1/5 of the maximum. This model was taken from Western Geophysical's depth-migration brochure.

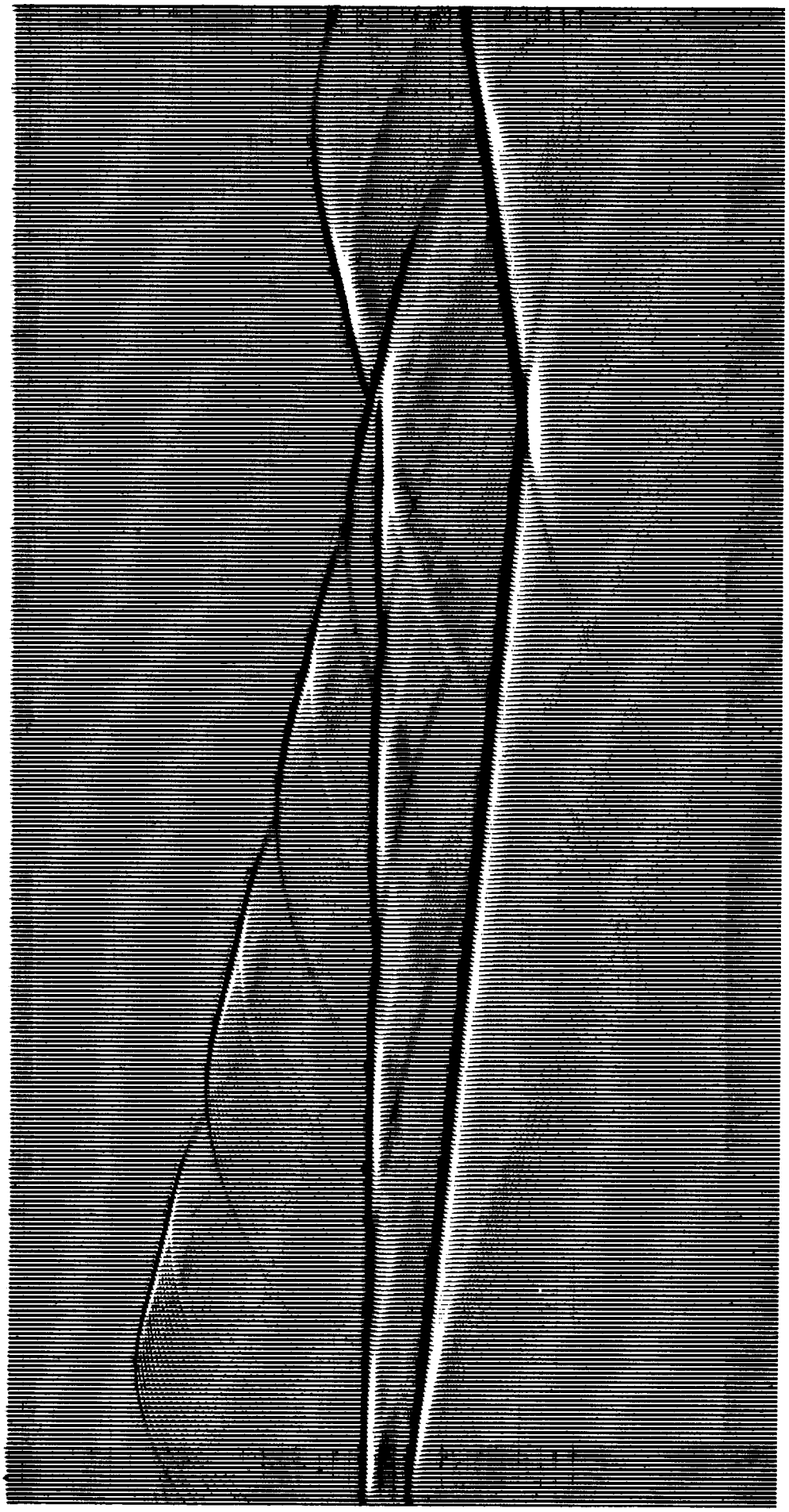

FIG. 6.10. Same results as in figure 6.3. but in order to more realistically simulate the bandwidth of real data the traces have been differentiated with respect to time. The broadening of the waveform, caused by anelasticity, is clearly shown. A gain proportional to $t^{3/2}$ was applied before plotting. The traces are clipped at 1/5 of maximum.

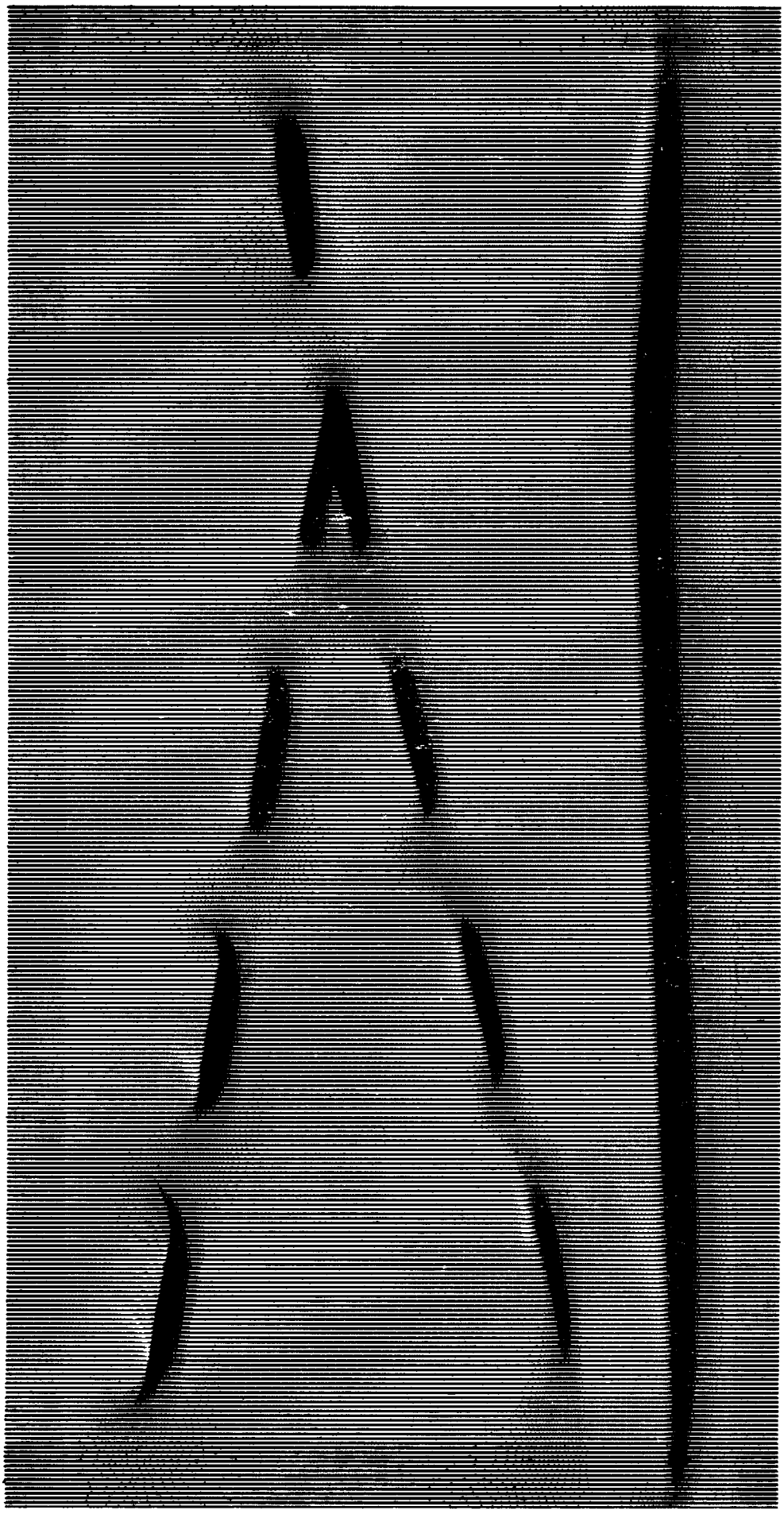

FIG. 6.11. The result of migrating the time section shown in figure 6.3. Total depth displayed is 4.4 km. The vertical smearing is mostly due to the fact that anelasticity was not included in the migration. Some of the lateral smearing is caused by dip-filtering (see Appendix B), and near the ends, absorption at the side boundaries. The plot is clipped at 1/3 of maximum.

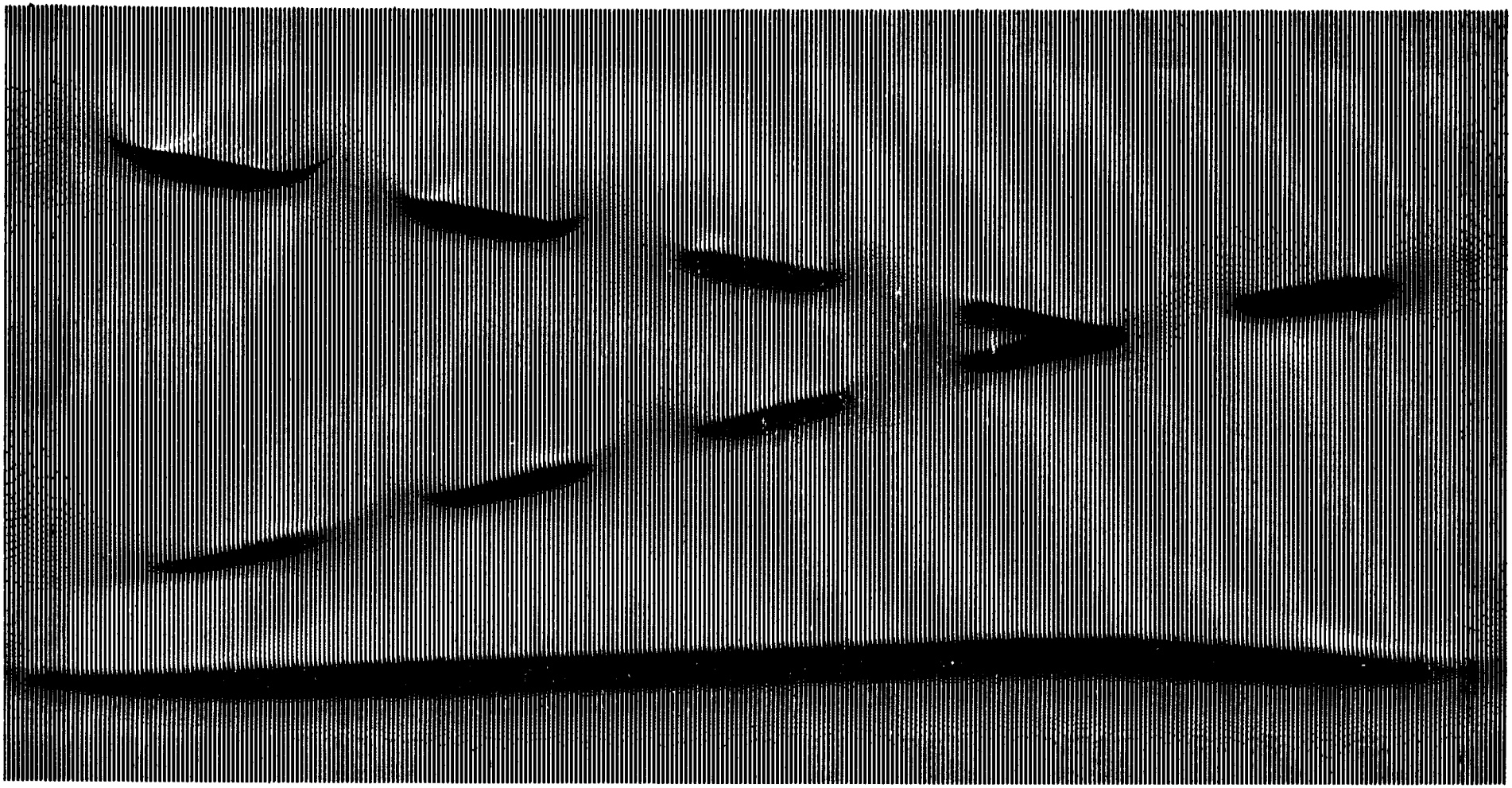

FIG. 4. (Kjartansson) The result of migrating the time section shown in figure 2. Total depth displayed is 4.4 km. The vertical smearing is mostly due to the fact that anelasticity was not included in the migration. Some of the lateral smearing is caused by the dip filtering, and near the ends, absorption at the side boundaries. The plot is clipped at 1/3 of maximum.

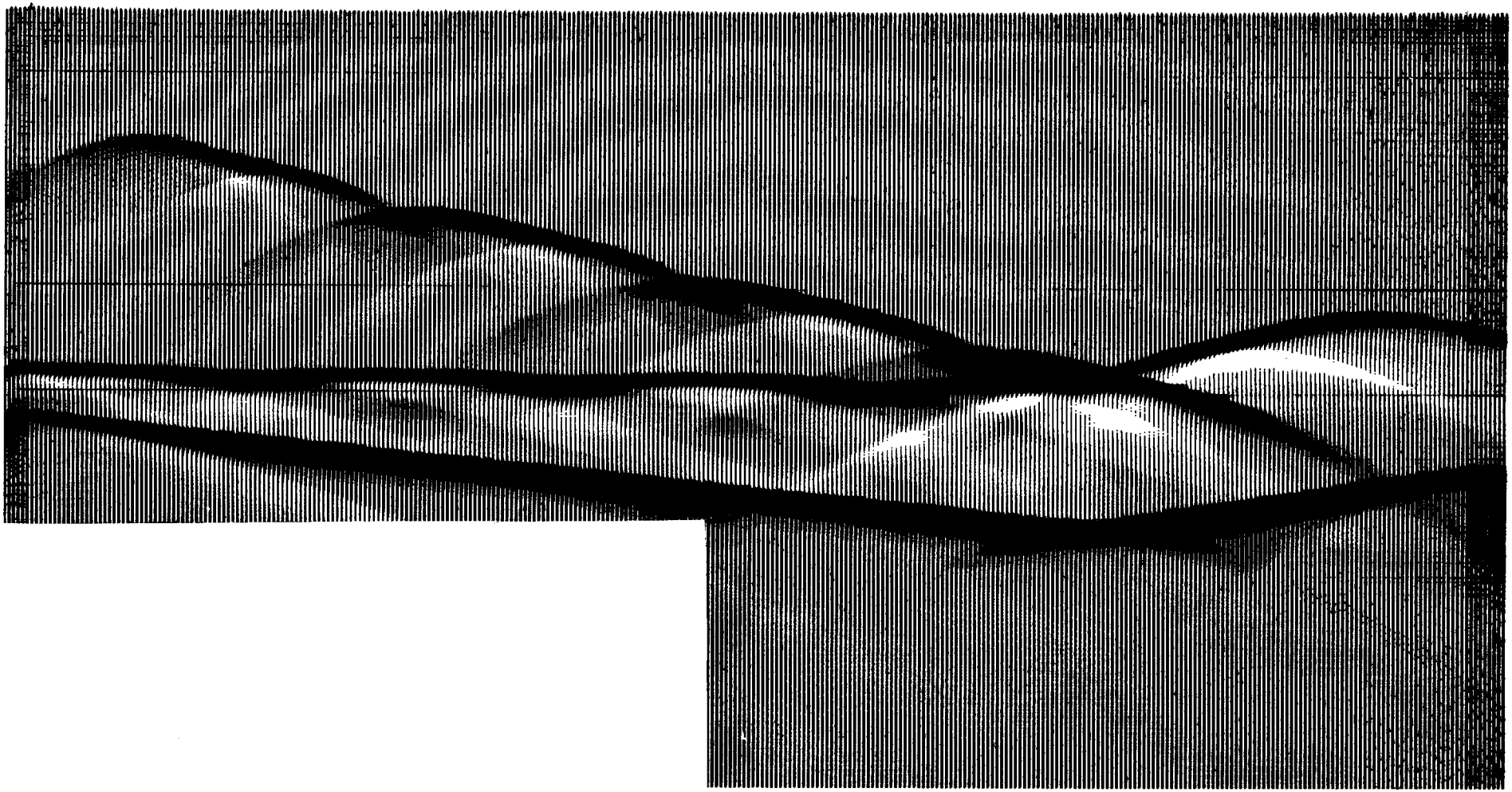

FIG. 2. (Kjartansson) A zero-offset section for the reflector and velocity structure shown, with $Q=40$. Total time displayed is four seconds. Velocities shown are for a reference frequency of approximately 1 Hz. The calculation included 330 traces, 320 depth steps and 512 complex frequencies or 1024 timepoints. A gain proportional to $t^{1/2}$ was applied before plotting. The traces are clipped to 1/5 of the maximum. This model was taken from Western Geophysical's Depth Migration brochure.